Development of the Swimbladder Surfactant System and Biogenesis of Lysosome-Related Organelles Is Regulated by BLOS1 in Zebrafish

Tianbing Chen,*,† Guili Song,* Huihui Yang,*,† Lin Mao,*,† Zongbin Cui,*,[1] and Kaiyao Huang*,[1]
*Institute of Hydrobiology, Chinese Academy of Sciences, Wuhan 430072, China and †University of Chinese Academy of Sciences, Beijing 100049, China

ABSTRACT Hermansky-Pudlak syndrome (HPS) is a human autosomal recessive disorder that is characterized by oculocutaneous albinism and a deficiency of the platelet storage pool resulting from defective biogenesis of lysosome-related organelles (LROs). To date, 10 HPS genes have been identified, three of which belong to the octamer complex BLOC-1 (biogenesis of lysosome-related organelles complex 1). One subunit of the BLOC-1 complex, BLOS1, also participates in the BLOC-1-related complex (BORC). Due to lethality at the early embryo stage in BLOS1 knockout mice, the function of BLOS1 in the above two complexes and whether it has a novel function are unclear. Here, we generated three zebrafish mutant lines with a BLOC-1 deficiency, in which melanin and silver pigment formation was attenuated as a result of mutation of *bloc1s1*, *bloc1s2*, and *dtnbp1a*, suggesting that they function in the same complex. In addition, mutations of *bloc1s1* and *bloc1s2* caused an accumulation of clusters of lysosomal vesicles at the posterior part of the tectum, representing a BORC-specific function in zebrafish. Moreover, *bloc1s1* is highly expressed in the swimbladder during postembryonic stages and is required for positively regulating the expression of the genes, which is known to govern surfactant production and lung development in mammals. Our study identified BLOS1 as a crucial regulator of the surfactant system. Thus, the zebrafish swimbladder might be an easy system to screen and study genetic modifiers that control surfactant production and homeostasis.

KEYWORDS lysosome-related organelles; Hermansky-Pudlak syndrome; surfactant system; swimbladder

LYSOSOME-RELATED organelles (LROs) are a collection of cell type-specific compartments that share some features with lysosomes, but with unique composition and morphology, and function in different processes (Huizing *et al.* 2008; Marks *et al.* 2013). Features that are shared between lysosomes and LROs include a low intraorganellar pH, some similar membrane proteins, and employing a common pathway of formation (Huizing *et al.* 2008). Examples of LROs include melanosomes in melanocytes and the retinal pigmented epithelium (RPE), delta granules in platelets, lytic granules in lymphocytes, and lamellar bodies in alveolar type 2 epithelial cells that function in pigmentation, hemostasis, immunity, and lung plasticity, respectively (Marks *et al.* 2013). Defects in LRO biogenesis have been found in some human genetic diseases, such as the Griscelli syndrome (GS), Chediak-Higashi syndrome (CHS), and Hermansky-Pudlak syndrome (HPS) (Huizing *et al.* 2008; Marks *et al.* 2013).

HPS is a group of phenotypically similar but genetically heterogeneous, autosomal recessive inherited disorders (Wei and Li 2013; Ammann *et al.* 2016). The common clinical features of HPS are hypopigmentation, reduced visual acuity, prolonged bleeding, and colitis. In some cases, pulmonary fibrosis, neuronal defects or immune deficiency are also present, depending on the different subtypes (Wei and Li 2013; Ammann *et al.* 2016). These symptoms are caused by abnormalities in tissue-specific LROs. Ten genes have been identified as causative genes for HPS, each of which corresponds to a HPS subtype, HPS1-10 (Wei and Li 2013; Ammann *et al.* 2016). The encoded proteins are main subunits in four lysosomal-trafficking protein complexes, including AP-3, and the biogenesis

doi: https://doi.org/10.1534/genetics.117.300621
Manuscript received December 11, 2017; accepted for publication January 8, 2018; published Early Online January 16, 2018.
Supplemental material is available online at www.genetics.org/lookup/suppl/doi:10.1534/genetics.117.300621/-/DC1.
[1]Corresponding authors: Institute of Hydrobiology, Chinese Academy of Sciences, Wuchang Donghu Nanlu 7#, Wuhan 430072, Hubei, China. E-mail: huangky@ihb.ac.cn; and Institute of Hydrobiology, Chinese Academy of Sciences, Wuhan 430072, Hubei, China. E-mail: zbcui@ihb.ac.cn

of three lysosome-related organelle complexes (BLOC-1, BLOC-2, and BLOC-3) (Wei and Li 2013; Ammann *et al.* 2016). At the cellular level, these complexes coordinately mediate protein trafficking in the endosomal system and regulate the biogenesis of LROs (Di Pietro *et al.* 2006; Salazar *et al.* 2006; Setty *et al.* 2007; Newell-Litwa *et al.* 2009; Bultema *et al.* 2012; Sitaram *et al.* 2012). Genes encoding subunits of these complexes that have not been found as HPS proteins are also thought to be putative HPS genes (Wei and Li 2013).

BLOC-1 is composed of eight distinct proteins (BLOS1, BLOS2, BLOS3, Dysbindin, Pallidin, Muted, Cappuccino, and Snapin) (Yang *et al.* 2012). Loss-of-function of Dysbindin, BLOS3, and Pallidin corresponds to HPS7-9 (Li *et al.* 2003; Morgan *et al.* 2006; Cullinane *et al.* 2011, 2012). Mutation of the subunits Muted and Cappuccino also cause HPS-like phenotypes in mice (Zhang *et al.* 2002; Ciciotte *et al.* 2003). However, dysfunction of the remaining three components (BLOS1, BLOS2, or Snapin) is embryonic lethal in mice, leaving their roles in HPS undetermined (Tian *et al.* 2005; Zhang *et al.* 2014; Zhou *et al.* 2016). These findings also imply potential novel functions of the three components beyond BLOC-1, which is supported by the discovery that BLOS1, BLOS2, and Snapin are also subunits of a newly identified complex, BLOC-1 related complex (BORC), which contains an additional five subunits named KXD1, myrlysin (LOH12CR1), lyspersin (C17orf59), diaskedin (C10orf32), and MEF2BNB (Pu *et al.* 2015). The BORC complex promotes kinesin-mediated "lysosome" (late endosomes and lysosomes) movement toward the cell periphery, and, hence, affects lysosome positioning in Hela cells, but the *in vivo* functions of this complex in vertebrates remain unclear (Pu *et al.* 2015). Snapin was first identified as a binding partner of SNAP-25 and functions in neurosecretion (Ilardi *et al.* 1999; Tian *et al.* 2005); it also attaches dynein to late endosomes, is essential for autophagy-lysosomal functions, and maintains synaptic activity in neurons (Cai *et al.* 2010; Di Giovanni and Sheng 2015). BLOS2 is a negative regulator of Notch signaling, and influences neural and hematopoietic stem and progenitor cell development by mediating the endolysosomal trafficking and degradation of Notch1; however, this function should be independent of BLOC-1 and BORC complexes since Notch1 levels were normal in mutants with the loss of other subunits within these two complexes (Zhou *et al.* 2016). BLOS1 interacts with SNX2 and TSG101 components from retromer and ESCRT-1 complexes, and mediates EGFR endosomal trafficking; however, this function is BLOC-1 dependent and is not the principal cause of lethality in mice since the same defects were detected in other nonlethal BLOC-1 mutants (Zhang *et al.* 2014). BLOS1 is also known as GCN5L1 (GCN5-like Protein 1)—a component of the mitochondrial acetyltransferase machinery that controls mitochondrial biogenesis and mitophagy (Scott *et al.* 2012, 2014; Webster *et al.* 2013). Interestingly, autophagosome accumulation has been reported in BLOS1/GCN5L1 knock-out MEF cells in two independent works (Scott *et al.* 2014; Zhang *et al.* 2014). This phenomenon also occurs in Snapin-KO mice (Cai *et al.* 2010), but it is absent in BLOS2-KO mice (Zhou *et al.* 2016). An impaired autophagy pathway has been suggested to be an important cause of lethality in BLOS1 and Snapin mutant mice (Zhang *et al.* 2014). In general, the functions of BLOS1 *in vivo* remain largely unknown, and thus its roles need to be further explored.

Zebrafish has become a popular model in the contexts of development and disease. The swimbladder is a specialized air-filled organ that regulates zebrafish buoyancy. The homology between the teleost swimbladder and tetrapod lung has long been recognized based on structural, topographic, and functional similarities (Cass *et al.* 2013). Molecular evidence further supports the evolutionary relationship between these two organs (Winata *et al.* 2009; Yin *et al.* 2011, 2012; Zheng *et al.* 2011). Early lung development is mediated by complex signaling and transcriptional programs, such as the WNT, SHH, FGF, and BMP pathways (Herriges and Morrisey 2014; Whitsett *et al.* 2015). Swimbladder morphogenesis in zebrafish is comparable to that of lung, and both SHH and WNT signaling are required for early swimbladder development (Winata *et al.* 2009; Yin *et al.* 2011). Moreover, zebrafish has been developed as a model of infection for the study of lung bacterial pathogens (López Hernández *et al.* 2015), and also studies in human fungal and mucosal infections (Gratacap *et al.* 2013; Voelz *et al.* 2015). More recently, the zebrafish swimbladder has been manipulated as an *in vivo* model to investigate neutrophilic inflammation for acute lung injury (Zhang *et al.* 2016). These studies demonstrate the potential value of the swimbladder for lung research.

A vital process for breathing during lung development is the establishment of the surfactant system. Pulmonary surfactant is a lipid:protein complex that lowers intra-alveolar surface tension to prevent terminal airway collapse at the end of expiration (Stahlman *et al.* 2000). It is composed of ~90% lipid, of which phosphatidylcholine (PC) is the main component, and four surfactant proteins (SP-A, SP-B, SP-C, and SP-D) (Goss *et al.* 2013). Surfactant is synthesized primarily by alveolar type 2 epithelial cells, where it is packaged into specialized organelles termed lamellar bodies through transporter ABCA3 (Cheong *et al.* 2007). Mature lamellar bodies secrete surfactant into the air spaces via exocytosis, where it unravels into tubular myelin that adsorbs and spreads at the air–liquid interface to form a film (Goss *et al.* 2013). A deficiency of pulmonary surfactant causes severe respiratory problems in neonates, children, and adults (Perez-Gil and Weaver 2010; Whitsett *et al.* 2010; Whitsett 2014; Whitsett and Weaver 2015; Olmeda *et al.* 2017). This system has a single evolutionary origin that predates the evolution of vertebrates and lungs (Daniels and Orgeig 2003). The secretion of surfactant from localized lamellar bodies at the caudal tip epithelium of the adult zebrafish swimbladder has also been observed (Robertson *et al.* 2014), implying a conserved cellular process of surfactant formation. However, systematic characterization of the surfactant system in zebrafish, and the molecular mechanisms that govern its formation, remain undescribed.

In this study, we generated zebrafish mutant lines carrying a BLOC-1 deficiency, and established new HPS animal models.

In contrast to the mouse models, neither significant impairments of the autophagy pathway nor obvious abnormalities of the nervous system were observed in *bloc1s1* and/or *bloc1s2* mutants. We demonstrated that deficiency of *bloc1s1* and *bloc1s2* resulted in abnormal positioning of lysosomal vesicles, which clustered at the posterior part of tectum. Moreover, we performed, for the first time, a detailed characterization of the surfactant system in zebrafish larvae. We explored the specific role of *bloc1s1* in control of the postembryonic development of the swimbladder and surfactant formation, likely by promoting a swimbladder-related transcriptional network.

Materials and Methods

Fish maintenance

Wild-type (WT) zebrafish (*Danio rerio*) (AB strain) and Tg (*fabp10a*:dsRed; *ela3l*:EGFP) lines were used (Korzh *et al.* 2008). All fish were maintained under standard conditions. Embryos were obtained through natural spawning.

Generation of mutant fish

bloc1s1, *bloc1s2*, *dtnbp1a*, and *tfeb* mutant lines were generated with the CRISPR/Cas9 system following established methods (Chang *et al.* 2013). Briefly, target sites were selected using the Zifit design Website (http://zifit.partners.org/), templates for guide RNAs were PCR-amplified and contained a T7 promoter and gRNA scaffold sequence, and sgRNAs were synthesized *in vitro* with T7 RNA polymerase (Thermo Scientific). The Cas9 capped mRNA was synthesized using the T7 mMESSAGEmMACHINE Kit (Ambion) and injected together with sgRNA into fertilized WT eggs.

RT-PCR and Q- PCR

Total RNA was extracted from zebrafish embryos with TRIzol reagent (Invitrogen) following the manufacturer's instructions. cDNA was synthesized with an oligo(dT)18 primer and the RevertAid first-strand cDNA synthesis kit (Thermo Scientific). SYBR green real-time PCR master mix (Bio-Rad) was used for Q-PCR. The RT-PCR and Q-PCR primers used are listed in Supplemental Material, Table S3 in File S1.

Whole-mount in situ hybridization (WISH)

Templates were PCR-amplified by adding a T7 promoter sequence to the primers (primers used are listed in Table S3 in File S1). RNA probes were generated by *in vitro* transcription and labeled with digoxigenin (DIG; Roche). Embryos were fixed overnight at 4° in 4% paraformaldehyde (PFA), dehydrated in 100% methanol, and stored at −20°. Before WISH, embryos were rehydrated for 5 min each in 75, 50, and 25% methanol diluted with PBST (1× PBS/0.1% Tween-20) and washed in PBST (5 × 5 min). Embryos were digested with proteinase K (10 μg/ml) and refixed with 4% PFA for 30 min, washed with PBST (5 × 5 min), and equilibrated in hybridization solution (50% formamide/5× SSC/0.1% Tween-20/ 50 μg/ml yeast transfer RNA/500 μg/ml heparin) for 5 hr at 68°. Embryos were then incubated in hybridization solution containing a probe overnight at 68°. Embryos were washed sequentially at 68° for 10 min each in 75, 50, and 25% post-hybridization solution (50% formamide/5× SSC/0.1% Tween-20) diluted with 2× SSC, 2× SSC (10 min at 68°), 0.2× SSC (2 × 30 min at 68°), 0.2× SSC:PBST (3:1, 1:1, 1:3, 0:1) (10 min each at room temperature). Embryos were blocked in blocking solution (PBST/2 mg/ml BSA/2% sheep serum) for 4 hr at room temperature, incubated in 1:3000 anti-DIG antibody (Roche overnight at 4°, washed with PBST (6 × 15 min) and coloration buffer (100 mM Tris-HCl/50 mM $MgCl_2$/100 mM NaCl/0.1% Tween-20) (3 × 5 min). Washed embryos were incubated with NBT-BCIP solution (Amresco) in the dark. When the staining was complete, the embryos were washed with PBST and imaged.

Transmission electron microscopy (TEM)

Zebrafish larvae were fixed in 2% glutaraldehyde at 4° overnight, washed with cacodylate buffer, postfixed in 1% OsO4 for 2 hr, washed with cacodylate buffer, placed in 1% uranyl acetate for 1 hr and dehydrated in ethanol. Larvae were then infiltrated through a propylene oxide/Epon series, embedded in Epon, and sectioned with an ultramicrotome (Leica). Sections were stained with uranyl acetate and lead citrate, and examined with a Hitachi HT-7700 electron microscope.

Melanin assay

Melanin determination was based on a published work (Maldonado *et al.* 2006). In brief, 20 larvae at each stage were pooled in 300 μl homogenization buffer (20 mM Tris-HCl, 2 mM EGTA, 1 mM PMSF) and homogenized. Following the addition of 500 μl 2 M NaOH, 100 μl DMSO, and 100 μl dH_2O, homogenates were incubated for 2 hr at 80° and then centrifuged. The absorbance of the supernatant at 350 nm was measured using a NanoDrop spectrophotometer. Samples were quantified by a melanin standard curve (melanin from *Sepia officinalis*; Sigma).

Histology, lysotracker red, and oil red O staining

Histological analysis was carried out as described (Malicki *et al.* 2011). Embryos were fixed overnight at 4° in 4% PFA and embedded with a JB-4 Kit (Polysciences). Blocks were cut into 4-μm sections and stained with hematoxylin.

For Lysotracker red staining, Lysotracker red (Beyotime) was diluted to a final concentration of 10 μM, added to an equal volume of fresh water on larvae, and incubated at 28° in the dark for 30 min. Larvae were then rinsed two to three times with fresh water and imaged.

For Oil Red O staining, the larvae were fixed in 4% PFA and then dehydrated in 100% methanol before use. Long-term storage in methanol would dissolve most lipids and leave only specific lipids in the surfactant to be stained. The 0.3% Oil Red O (Sigma) in 60% 2-propanol was freshly made and filtered. Larvae were whole-mount stained or embedded in optimum cutting temperature compound (OCT) and sectioned (30 μm) before staining.

Western blotting and immunohistochemistry

Larvae were lysed (2 μl per embryo) in cold RIPA cell lysis buffer (Beyotime) containing complete protease inhibitor Cocktail (Roche). Lysates were incubated on ice for 30 min and then centrifuged at 4° to pellet the cellular debris. Samples were boiled at 95° for 10 min with SDS sample buffer, loaded onto a 15% polyacrylamide gel, and transferred to PVDF membranes. Blots were incubated with primary antibodies (anti-LC3; 1:1000; Proteintech; anti-actin 1:500; Sigma), followed by HRP-conjugated secondary antibodies. Signals were quantified by densitometry.

For immunohistochemistry, larvae were fixed in 4% PFA in PBS for 2 hr at room temperature, cryoprotected in 30% sucrose at 4° overnight, embedded in OCT and sectioned at −20°. Sections (20 μm) mounted on slides were fixed in ice-cold acetone for 2 min, and stored at −20°. Slides were thawed, air-dried, washed three time with PBS and blocked. Sections were then incubated with anti-LC3 (1:50) for 4 hr at 4°, washed, incubated with secondary antibody, and imaged with confocal microscopy (SP8; Leica)

Morpholino phenocopy and transgenic rescue

A morpholino antisense oligonucleotide was designed against the ATG region of the *bloc1s1* mRNA (*bloc1s1*-ATG-MO: AAG TAGCCAAAATGCTCTCGCGGTT). The morpholino was then injected into one-cell stage WT embryos at different concentrations. The transgenic rescue experiment was conducted as previously described (Hugo *et al.* 2012).

Statistical analyses

The *t*-test between paired samples (wild type *vs.* mutant) was performed using Excel (Microsoft, Redmond, WA).

Data availability

The authors state that all data are represented fully within the article. Strains used are available upon request. Supplemental Materials contain the Figures S1–S5 and Tables S1–S3 in File S1.

Results

Conservation of BLOS1-containing complexes among vertebrates, and the expression pattern of bloc1s1 during early zebrafish development

To illuminate the potential conserved function of BLOS1 among vertebrates, we first compared the similarity of all BLOC-1 and BORC subunits among zebrafish, mice, and humans. Excluding *DTNBP1* (which is duplicated in the zebrafish genome, *dtnbp1a*, and *dtnbp1b*), the zebrafish genome contains a single copy of each gene encoding subunits of the BLOC-1 and BORC complex; the amino acid identity between zebrafish and their human counterparts ranged from 34.4 to 89.6% (Table S1 in File S1), indicating the two complexes are highly conserved among vertebrates. Compared with *dtnbp1a*, the protein encoded by *dtnbp1b* is truncated and displays lower amino acid identity. Thus, the protein encoded by *dtnbp1a* is much more likely to be the subunit of BLOC-1 in zebrafish (Table S1 in File S1).

BLOS1 is the most conserved subunit, and it shares 89.6% amino acid identity with human BLOS1 (Figure 1A and Table S1 in File S1). The temporal and spatial expression pattern of the *bloc1s1* gene during embryogenesis was first examined by RT-PCR in zebrafish embryos. The *bloc1s1* transcript is maternally stored, and its expression was detected throughout development up to 120 hours postfertilization (hpf; Figure 1B). To determine where *bloc1s1* might function during embryogenesis, we conducted whole-mount *in situ* hybridization. Generally, *bloc1s1* was ubiquitously expressed at earlier stages up to 72 hpf, when relatively high expression was detected in a specific area of the brain (Figure 1C). At 4 and 5 days postfertilization (dpf), *bloc1s1* transcript showed similar patterns, with high expression levels in the inner ear, gut, and in the pneumatic duct and swimbladder (Figure 1C).

Mutation of bloc1s1 resulted in multi-systemic defects in zebrafish

To investigate the function of *bloc1s1*, we generated *bloc1s1* mutant zebrafish with the CRISPR/Cas9 system (Chang *et al.* 2013). Two mutant alleles were obtained from different P0 founders by targeting exon 2 of the *bloc1s1* gene. One has a 4-bp deletion in exon 2 (designated $bloc1s1^{ihb816}$), and the other harbors a 17-bp deletion that includes the splicing donor (SD) site between exon 2 and intron 2 (designated $bloc1s1^{ihb815}$) (Figure 2A). At the cDNA level, the $bloc1s1^{ihb816}$ allele resulted in the same 4-bp deletion in the coding region, while the $bloc1s1^{ihb815}$ allele acquired a new splicing donor site within intron 2 and formed a chimeric transcript (Figure S1A in File S1). Both alleles resulted in a frameshift after the target site, and the presumptive proteins were truncated (Figure 2B and Figure S1B in File S1). The relative mRNA expression level was also significantly reduced in homozygotes of $bloc1s1^{ihb815}$ or $bloc1s1^{ihb816}$ embryos (Figure 2C), likely through a nonsense-mediated decay mechanism (Wittkopp *et al.* 2009).

Heterozygous $bloc1s1^{ihb815/+}$ or $bloc1s1^{ihb816/+}$ fish are viable, have no discernable phenotype, and develop into fertile adults. Homozygous mutants obtained from a cross between either $bloc1s1^{ihb815/+}$ or $bloc1s1^{ihb816/+}$ heterozygotes did not show any observable phenotype at early stages. Up to 3 dpf, when iridophores are formed in the eye and body in wild-type larvae, iridophores contain vesicular organelles containing guanine crystals, also termed silver pigment, which give them reflective properties under reflective light (Schonthaler *et al.* 2007; Figure 2, E, G, I, and K). These light reflections were consistently absent in *bloc1s1* mutants (Figure 2, F, H, J, and L); however, this phenotype was not caused by the absence of iridophores since $bloc1s1^{ihb815}$ showed a normal iridophore development and distribution (Figure 2I); moreover, since iridosomes occupied large spaces in the cells, absence of these organelles resulted in iridiphores with much smaller size in *bloc1s1* mutants (Figure S1C in File S1). Hypopigmentation

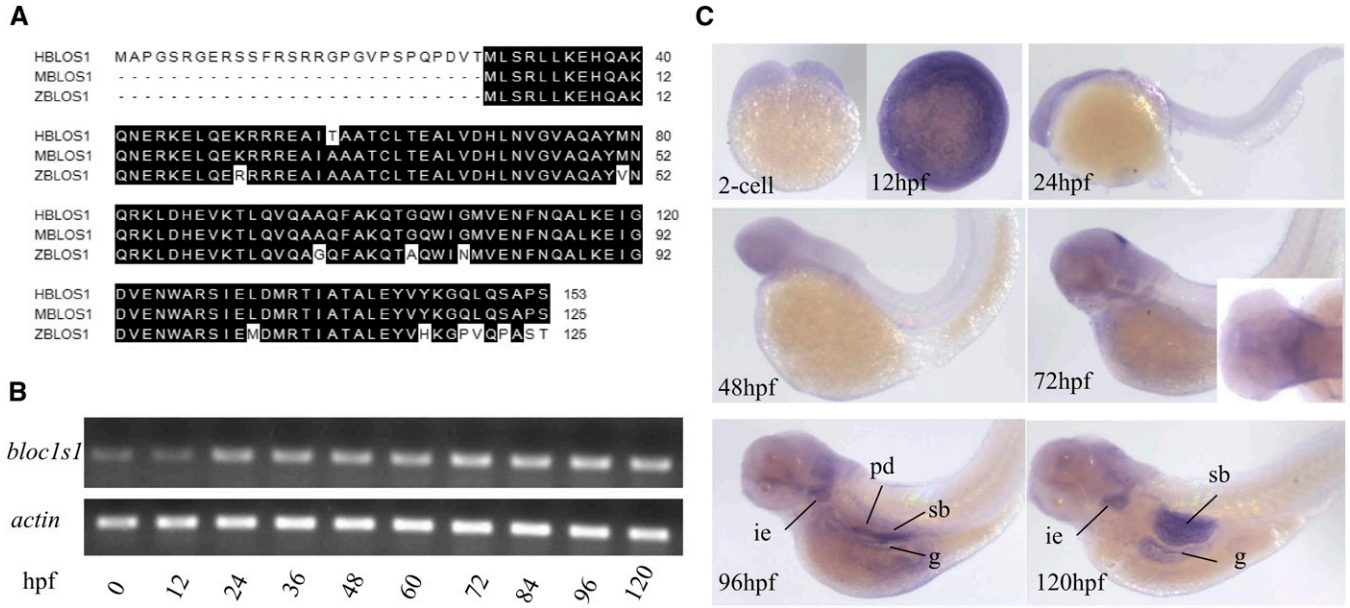

Figure 1 Expression of *bloc1s1* mRNA during zebrafish embryogenesis. (A) Sequence alignment of BLOS1 from human, mouse, and zebrafish. (B) Expression patterns of *bloc1s1* at different stages were analyzed by RT-PCR, with *β-actin* as the control. (C) Detection of *bloc1s1* transcript by whole-mount *in situ* hybridization. Inset at 72 hpf shows a dorsal view image. hpf, hours postfertilization; ie, inner ear; pd, pneumatic duct; sb, swimbladder; g, gut.

of skin melanocytes could also be observed in homozygotes starting from 3 dpf (Figure 2H); total melanin levels in *bloc1s1*^{ihb815} or *bloc1s1*^{ihb816} decreased significantly compared with WT (Figure 2D). In addition to the pigment phenotype, *bloc1s1*^{ihb815}/*bloc1s1*^{ihb816} showed neither any malformations nor reduced viability during the first 4 days. A slight absorption delay and deflation of the swimbladder were observed at 5 dpf (Figure 2L). Starting from 7 dpf, the mutant larvae developed an enlarged liver with progressive necrosis (Figure S1, D and E in File S1); Crossing of the *bloc1s1*^{ihb815} allele into a Tg (*fabp10a*:dsRed; *ela3l*:EGFP) background also revealed progressive degeneration of the pancreas (Figure S1F in File S1); These late-stage phenotypes were accompanied by a great reduction of viability and resulted in homozygotes death between 7 and 15 dpf. Since *bloc1s1*^{ihb815} and *bloc1s1*^{ihb816} larvae showed exactly the same phenotypes, only *bloc1s1*^{ihb815} were chosen for further analysis.

Impairments of pigment granule formation in bloc1s1 mutant zebrafish

Since BLOS1 is a subunit of BLOC-1 that mediates the biogenesis of pigment granules in mammals and fly (Li *et al.* 2004; Wei and Li 2013), we speculated that the pigment phenotypes in *bloc1s1*^{ihb815} might be the result of defective biogenesis of pigment granules. We compared the structure of melanosomes in retinal pigmented epithelium (RPE) from *bloc1s1*^{ihb815} *vs.* WT using TEM. The zebrafish melanosome initiates biogenesis with a round shape containing multivesicle bodies, while the mature melanosome is larger and ellipsoid (Daly *et al.* 2013). Both round and ellipsoid melanosomes were detected in WT RPE (Figure 3, A, C, and E). However, the melanosomes from *bloc1s1*^{ihb815} RPE were mainly round, and ellipsoid melanosomes were substantially absent at all stages (Figure 3, B, D, and F). Consistent with their appearance in the immature state, the melanosomes from *bloc1s1*^{ihb815}contained many vesicle-like structures (Figure 3H), resembling the immature melanosomes documented in the literature (Daly *et al.* 2013). In contrast, the lumen of melanosomes from WT had a solid appearance, corresponding to the mature state (Figure 3G); the round melanosomes in WT may result from the cross-section of mature melanosomes with a different orientation, instead of immaturation. Because they are blocked in the immature state, the average area of melanosomes in *bloc1s1*^{ihb815} were reduced at all stages examined (Figure 3I). The density of the melanosomes was not reduced at 3 and 5 dpf in *bloc1s1*^{ihb815} compared with WT larvae, although this value was reduced at 7 dpf (Figure 3J). Together, these results indicated that the maturation process, but not the initial steps of melanosome biogenesis, was defective after *bloc1s1* mutation. The decrease in melanosome density at 7 dpf in *bloc1s1*^{ihb815} was likely due to the degeneration of the melanosomes themselves.

We also detected iridosomes in WT zebrafish (Figure 3K); these organelles were absent in *bloc1s1*^{ihb815} larvae (Figure 3L), implying that the initiation of iridosome biogenesis was completely blocked.

No detectable autophagy-related abnormalities in bloc1s1 mutant zebrafish

Abnormal autophagy activity was thought to be an important cause of lethality in BLOS1-KO mice (Zhang *et al.* 2014), which resulted from a positive influence on transcription factor EB (TFEB)—a master regulator of autophagy (Settembre *et al.* 2011; Scott *et al.* 2014). Therefore, we examined autophagy

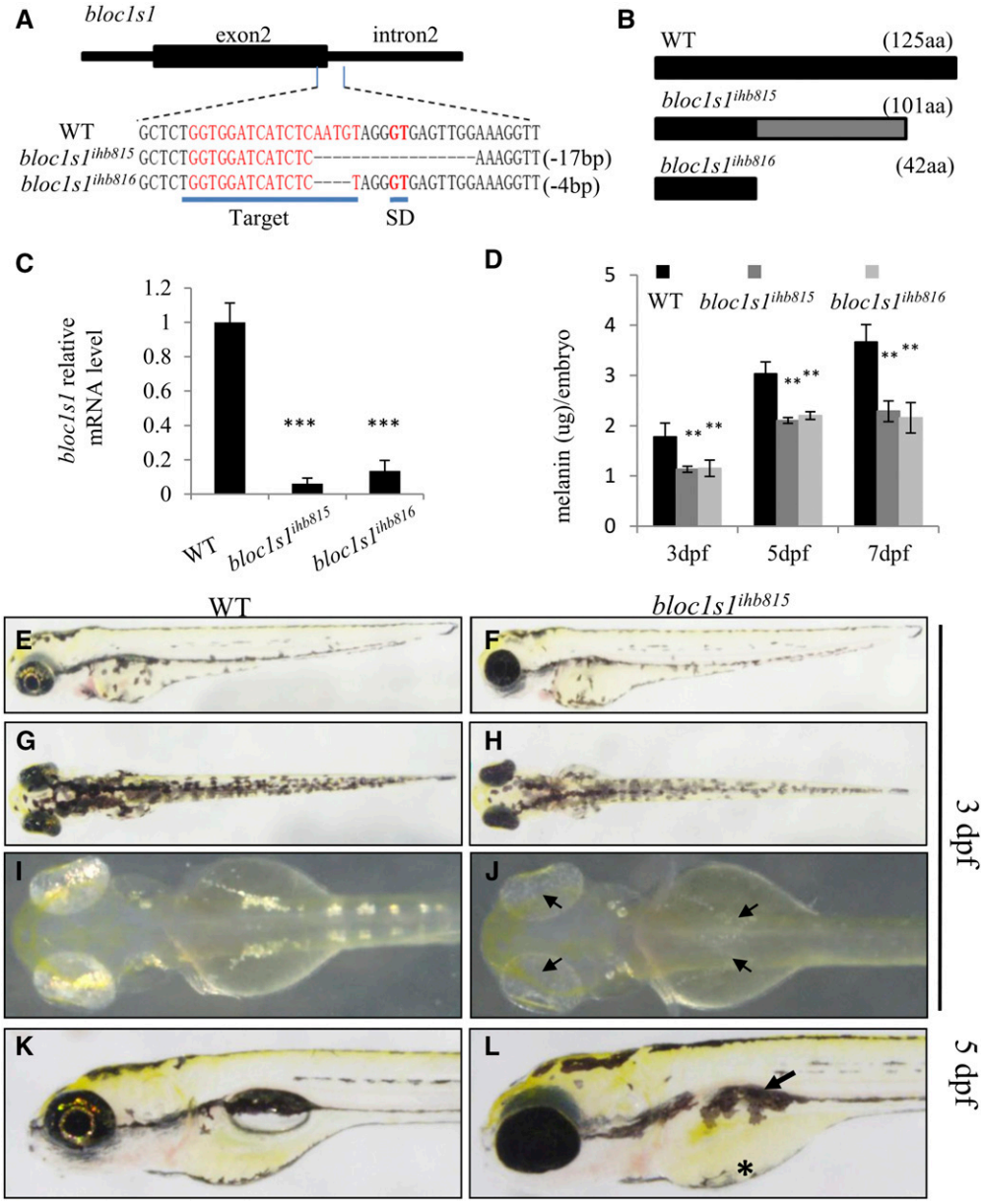

Figure 2 Mutation of *bloc1s1* causes multi-developmental defects in zebrafish. (A) Top panel: the schematic diagram shows the structure of the target region of the *bloc1s1* gene. Black box, exon; solid line, introns. The bottom panel shows a comparison of the genomic DNA sequences among WT and two mutant alleles, *bloc1s1*^{ihb815} (with a 17-bp deletion) and *bloc1s1*^{ihb816} (with a 4-bp deletion). The target sequence is indicated in red and underlined; SD, splicing donor. (B) Schematic structures of WT and truncated BLOS1 proteins. (C) The relative mRNA levels of *bloc1s1* in WT and homozygous mutants were assayed by Q-PCR at 5 dpf. The results are expressed as the mean ± SEM of three independent experiments (*** $P < 0.001$; *t*-test) (D) The melanin levels in *bloc1s1* mutants were significantly lower than in WT from 3 to 7 dpf. The results are expressed as the mean ± SEM of four independent experiments (** $P < 0.01$; *t*-test). (E–H) Bright-field images show the hypopigmentation of skin melanocytes and absence of iridophore reflections in *bloc1s1* mutants. The completely dark eyes in *bloc1s1* mutants resulted from the loss of reflections from iridophores. (I and J) Dark-field images show an absence of iridophore reflections instead of the iridophores themselves in skin and eye (arrowheads) of *bloc1s1* mutants pretreated with PTU to block melanin synthesis. (K and L) The 5 dpf *bloc1s1* mutants show a deflated swimbladder (arrowhead) and a delay in yolk absorption (asterisk).

activity in *bloc1s1*^{ihb815} by assessing the expression level of LC3, which is a robust marker of autophagosomes; the cytoplasmic form of LC3 (LC3I) is converted into an autophagosomal membrane-bound form of LC3 (LC3II) through cleavage and lipidation after induction of autophagy (Boglev *et al.* 2013). Unexpectedly, the protein level of LC3II in *bloc1s1*^{ihb815} was comparable to that in their WT siblings at 3.5 and 4.5 dpf (Figure S2, A and B in File S1), implying that there was no change in general autophagy activity in *bloc1s1*^{ihb815}. However, it is possible that the BLOS1-TFEB axis only functions in specific cell types rather than affecting the whole body. To assess the potential contribution of this axis to the lethal phenotype of *bloc1s1*^{ihb815}, we also established a *tfeb* mutant line, which showed no influence on development, but with a lower survival ratio when they grow up to become adults (Figure S3, C–E in File S1). The *bloc1s1*^{ihb815} : *tfeb*^{ihb817} double mutant did not show any new phenotype or altered survival curves when compared with *bloc1s1*^{ihb815} (Figure S3F in File S1). These data demonstrated that the BLOS1-TFEB axis did not contribute to the lethal phenotype in *bloc1s1*^{ihb815}.

Accumulation of lysosomal vesicle clusters at the posterior part of the tectum in bloc1s1 mutant zebrafish

BLOS1 is also a subunit of BORC that regulates lysosome positioning in HeLa cells (Pu *et al.* 2015). To examine the effect on lysosome positioning after *bloc1s1* mutation in zebrafish, we employed Lysotracker red to stain the lysosomes *in vivo* in series of embryo stages (Sasaki *et al.* 2014). The *bloc1s1*^{ihb815} larvae showed similar staining patterns to their WT siblings during the first 4 days. However, beginning at 5 dpf, a specific accumulation of signals was observed at the posterior part of the tectum in *bloc1s1*^{ihb815}, and these signals

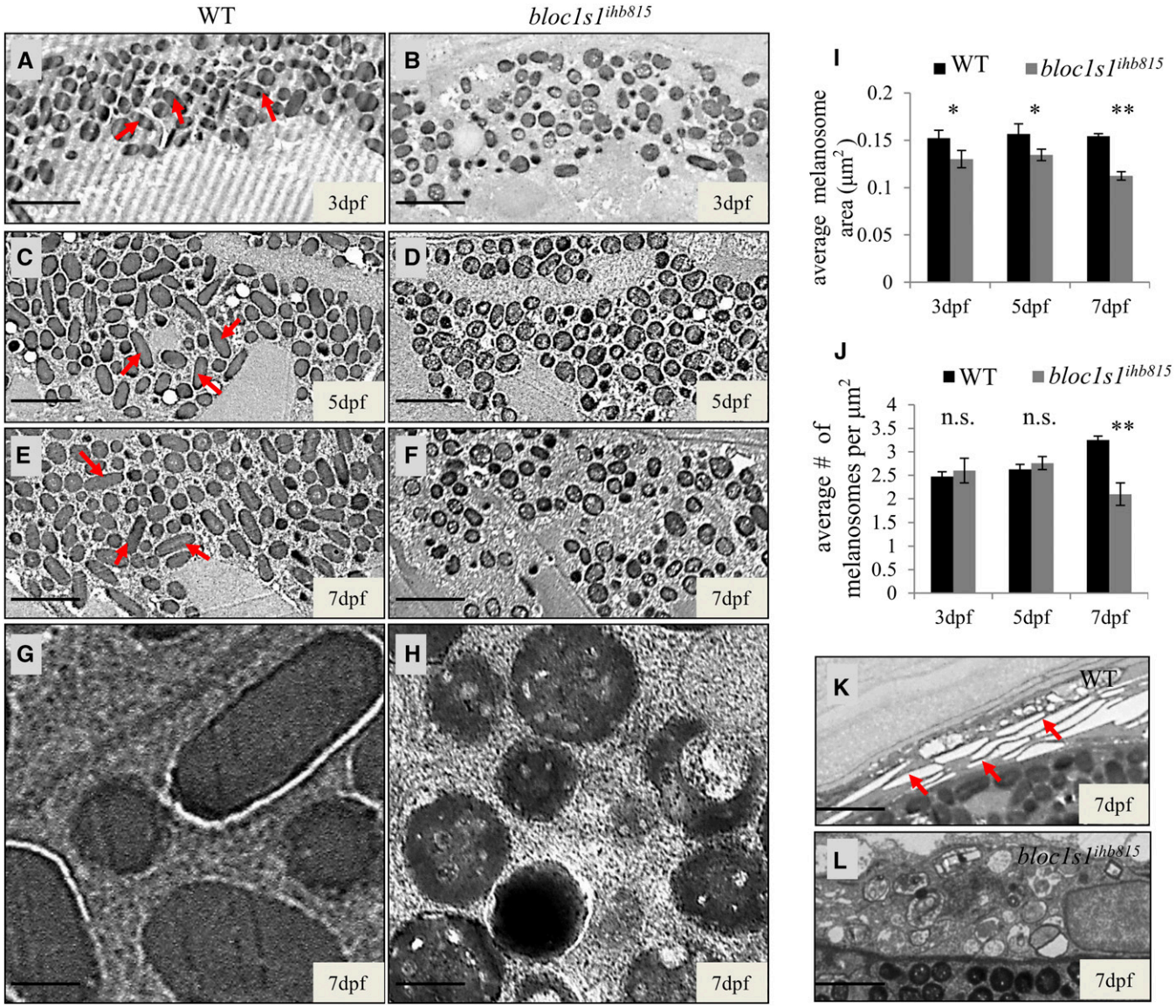

Figure 3 Impairments of pigment granule formation in *bloc1s1*^{ihb815} zebrafish. (A–F) TEM reveals an abnormal morphology of melanosomes within the *bloc1s1*^{ihb815} RPE (B, D, and F) as compared to their WT siblings (A, C, and E) from 3 to 7 dpf (Bar, 2 μm). Arrowheads denote typical mature melanosomes with an ellipsoid shape in WT zebrafish. (G and H) Magnified images reveal that the immature melanosomes from *bloc1s1*^{ihb815} RPE (H) contain many vesicles. The lumen of mature melanosome has a solid appearance in WT zebrafish (G) (Bar, 250 nm). (I) The average area of melanosomes is smaller in the *bloc1s1*^{ihb815}. (J) The average densities of melanosomes in a 25-μm^2 area of the RPE is comparable between WT and *bloc1s1*^{ihb815} larvae at 3 and 5 dpf but becomes lower in *bloc1s1*^{ihb815} at 7 dpf. The results (I and J) are expressed as the mean ± SEM of three independent experiments (n.s., not significant; ** $P < 0.001$; *t*-test). (K and L). The space in WT iridophores is occupied by iridosomes (K, arrowheads), which are absent in *bloc1s1*^{ihb815} larvae (L) (Bar, 2 μm). The lumen of iridosomes appears hollowed as the reflective crystalline material is lost during sectioning.

were consistently observed during the following stages (Figure 4, A and B). Since autophagosomes in zebrafish fuse with lysosomes and form an acidic luminal environment, which can also be detected using Lysotracker red (Sasaki *et al.* 2014), we performed immunostaining to determine the nature of these signals. However, these Lysotracker red-positive structures were not stained with LC3 antibody, indicating that they were not autophagosomes (Figure 4C). We further performed TEM and obtained better resolution of these Lysotracker red-positive structures. As shown in Figure 4, E and E′, they showed irregular morphologies. Most were vesicle clusters resembling perinuclear lysosome clusters in HeLa cells with a BORC deficiency (Pu *et al.* 2015). These data suggested that *bloc1s1* was required for the normal positioning of these lysosomal vesicles at the posterior part of the tectum in zebrafish.

Phenotypes comparison of BLOC1 deficiency models with different mutational subunits

We also generated additional BLOC-1 deficiency models, including *bloc1s2* and *dtnbp1a*. We had previously reported a *bloc1s2* mutant line that contained a 4-bp insertion and only destroyed three out of the four *bloc1s2* transcripts in zebrafish,

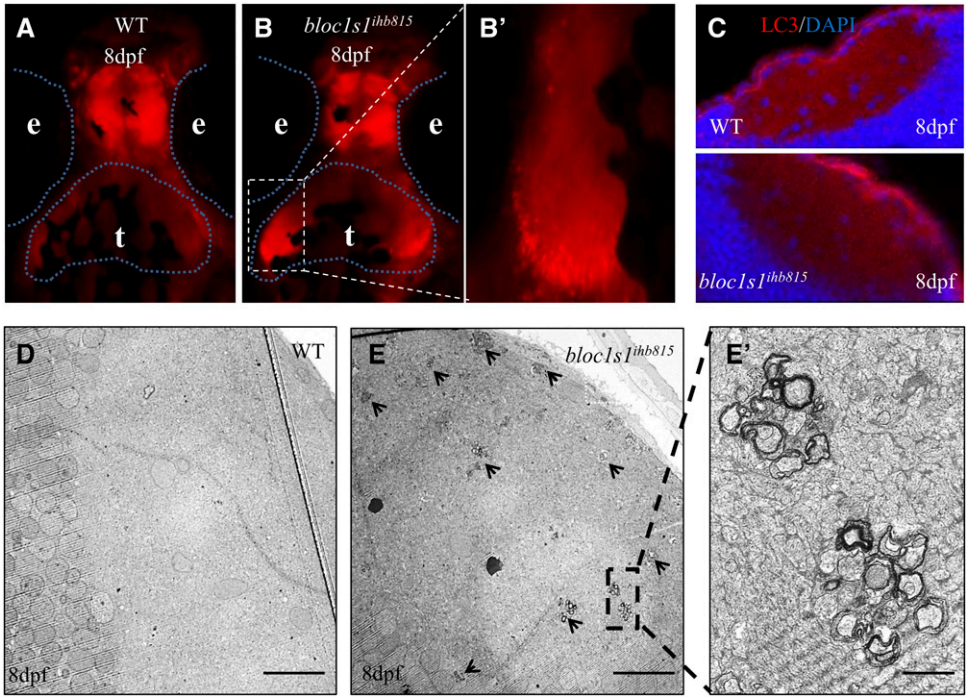

Figure 4 Accumulation of Lysotracker-positive signals at the posterior part of the tectum in *bloc1s1*^{ihb815} zebrafish. (A and B) Dorsal view of Lysotracker staining reveals a specific accumulation of punctate signals at the posterior part of the tectum in *bloc1s1*^{ihb815} larvae (B and B′), as compared to wild type (A). Dotted lines outlined e (eye) and t (tectum). (C) Representative images of continuous transverse sections (20 μm) through the tectum region of wild-type (top) and *bloc1s1*^{ihb815} larvae (bottom) stained with DAPI to detect nucleus and LC3 antibody to detect LC3II-containing autophagosomes (negative). (D and E) TEM images of the posterior part of the tectum (Bar, 10 μm). The punctate signals in *bloc1s1*^{ihb815} larvae (E, arrowheads) are composed of vesicles in clusters (E′, Bar, 1 μm).

making it a hypomorphic mutant (*bloc1s2 hypo*) (Zhou *et al.* 2016). Here, we changed the target and obtained a new mutant allele, *bloc1s2*^{ihb818}, that contained a 29-bp deletion and resulted in the disruption of all four transcripts (Figure S3, A and C in File S1). The mutant allele, *dtnbp1a*^{ihb819}, contained a 2-bp deletion in exon 2 of the *dtnbp1a* gene (Figure S3, B and D in File S1). Both mutant alleles caused frameshift mutation, and the presumptive proteins were truncated (Figure S3, E and F in File S1).

The abnormal phenotypes of *bloc1s2*^{ihb818} or *dtnbp1a*^{ihb819} larvae were recognized from 3 dpf, when the reflection of iridophores was greatly reduced compared with their WT siblings. From dorsal view, the reflection of iridophores from body and eyes was missing in both *bloc1s2*^{ihb818} and *dtnbp1a*^{ihb819}; however, this light reflection was retained on eyes from a lateral perspective (Figure 5A). The *bloc1s2 hypo* larvae did not show this phenotype, indicating that the remaining transcript was necessary and sufficient to maintain this feature. The melanin levels also decreased, but to a divergent degree in *bloc1s2*^{ihb818} and *dtnbp1a*^{ihb819}, and their reduction was weaker than that in *bloc1s1*^{ihb815} (Figure 5B). The melanin levels in *bloc1s2*^{ihb818} were lower than in WT at a series of stages, although they did not show statistical significance compared with WT (Figure 5B). *dtnbp1a*^{ihb819} : *bloc1s1*^{ihb815} double mutants did not develop a distinguishable pigment phenotype when compared with *bloc1s1*^{ihb815} (data not shown). All these data demonstrated that *bloc1s1*, *bloc1s2*, and *dtnbp1a* were all required for the pigmentation of zebrafish, suggesting that they function in the same pathway as the BLOC-1 complex.

Interestingly, *bloc1s2*^{ihb818} also accumulated specific Lysotracker-positive signals at the posterior part of tectum, which occurred at the same time as that in *bloc1s1*^{ihb815} (Figure 5C). However, these signals were absent in *dtnbp1a*^{ihb819}, indicating that the phenotype was only related to *bloc1s1* and *bloc1s2*, but excluded from *dtnbp1a* (Figure 5C). Since their coding proteins, BLOS1 and BLOS2, are both subunits of BORC (Pu *et al.* 2015), we proposed that this phenomenon represented a tissue-specific function of BORC in regulating lysosomal vesicle positioning in zebrafish.

Both *bloc1s2*^{ihb818} and *dtnbp1a*^{ihb819} mutants can survive to adulthood, although with poor growth and low survival rates. The late-stage phenotypes in *bloc1s1*^{ihb815}, including deflation of the swimbladder, hepatomegaly, and pancreas degeneration, were all absent in *bloc1s2*^{ihb818} and *dtnbp1a*^{ihb819}. Thus, these late-stage phenotypes were *bloc1s1*-specific and should be independent of the BLOC-1 and BORC complexes.

Functions of bloc1s1 in the surfactant system of the swimbladder

To investigate the cause of the defect in the swimbladder in *bloc1s1*^{ihb815}, we first analyzed swimbladder development using tissue-specific markers including *hb9* (epithelium), *fgf10a* (mesenchyme), and *elovl1a* (mesothelium) (Winata *et al.* 2009; Yin *et al.* 2011). We used 3.5-dpf larvae since *bloc1s1*^{ihb815} could be definitely distinguished at this time. We found that the transcripts of all three markers remained in the swimbladder at this stage, but their expression was reduced in *bloc1s1*^{ihb815} (Figure 6A). To determine to what extent this phenomenon might reflect the developmental alterations of the swimbladder, we performed a histological analysis at several stages. However, the global architecture of *bloc1s1*^{ihb815} did not show abnormalities at 4 dpf when compared with their WT siblings (Figure 6B). However, the epithelium thickened and the whole swimbladder wall seemed to be compact at 6.5 dpf (Figure 6B).

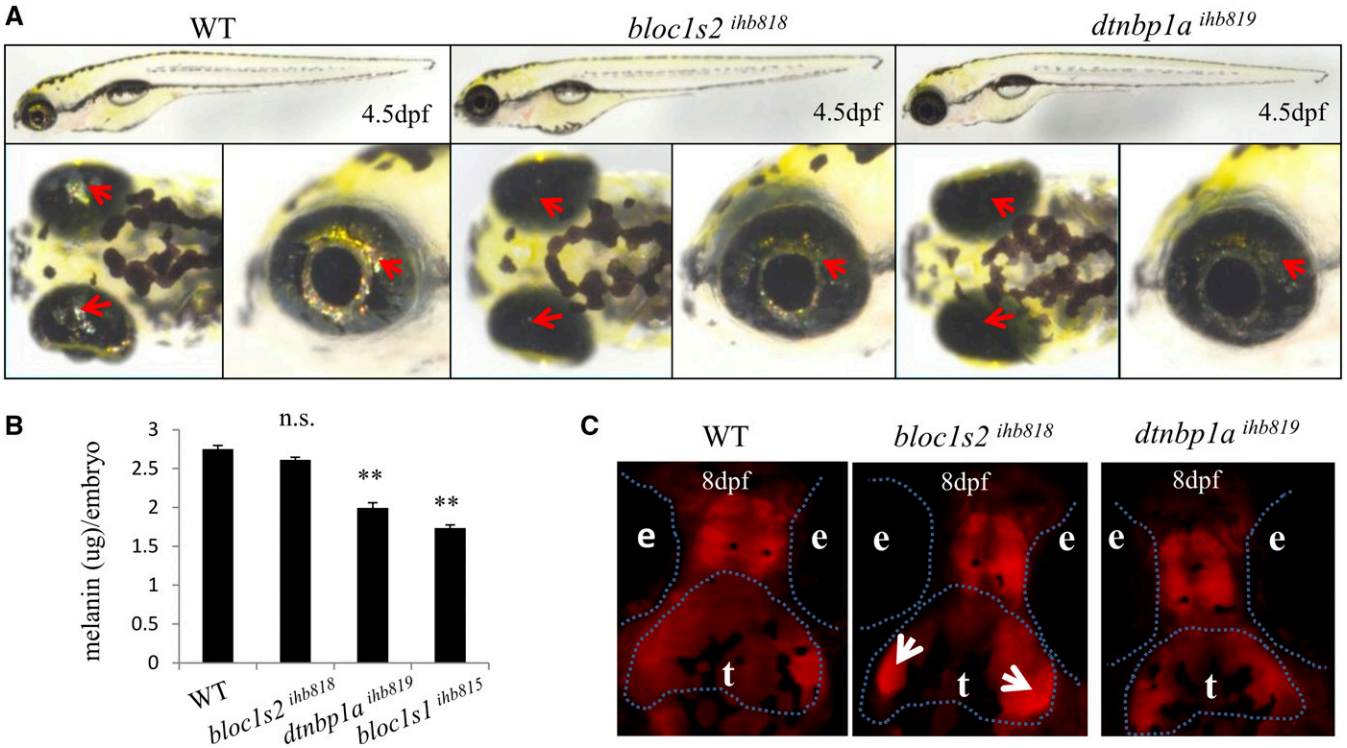

Figure 5 Comparison of the phenotypes of BLOC-1 deficiency in zebrafish. (A and B) Pigment defects in *bloc1s2*^{ihb818} and *dtnbp1a*^{ihb819} larvae at 4.5 dpf. Bright-field images show the decrease in iridophore reflections in *bloc1s2*^{ihb818} and *dtnbp1a*^{ihb819} larvae (A, red arrowheads). The melanin levels in *bloc1s2*^{ihb818} and *dtnbp1a*^{ihb819} are lower than in WT but higher than in *bloc1s1*^{ihb815} larvae at 4.5 dpf and do not show statistical significance between WT and *bloc1s2*^{ihb818} larvae (B). The results are expressed as the mean ± SEM of four independent experiments; n.s., not significant; ** $P <$ 0.001; *t*-test. (C) Dorsal view of Lysotracker *in vivo* staining revealing a specific accumulation of punctate signals at the posterior part of the tectum in *bloc1s2*^{ihb818} (white arrowheads), but not in *dtnbp1a*^{ihb819}. Dotted lines outlined e (eye) and t (tectum).

Most of the *bloc1s1*^{ihb815} larvae were unable to inflate their swimbladder, but a few of them displayed a semi-inflated swimbladder at ~5 dpf (Figure 6C). After careful observation and counting, we found that >90% of the *bloc1s1*^{ihb815} larvae possessed air bubbles at ~5 dpf—a period when zebrafish larvae first inflate their swimbladder. However, these air bubbles formed and disappeared quickly, and they occurred at only ~5 dpf, making them difficult to notice. The bubbles were either present in the swimbladder or in the intestine, likely due to the difficulty associated with gas delivery to the swimbladder. This initially ignored phenomenon implied that *bloc1s1*^{ihb815} had normal gas delivery to the swimbladder.

Since both the general architecture and gas delivery seemed normal in *bloc1s1*^{ihb815}, we investigated the cause of the swimbladder deflation. The surfactant system provided inspiration because it has been proposed to exhibit antiadhesive functions that prevent the adhesion of adjacent epithelial surfaces in nonmammals (Daniels and Orgeig 2003). Therefore, we attempted to compare the surfactant system in both WT and *bloc1s1*^{ihb815} larvae with Oil Red O, which has been extensively used to stain lipids in zebrafish (Hugo *et al.* 2012; Gu *et al.* 2014). The surfactant system could also be stained (Hugo *et al.* 2012). The surfactant system in WT larvae started the formation process at ~3.5 dpf, and was already well developed at 4.5 dpf, immediately before swimbladder inflation (Figure 6D). This staining was maintained at late stages, supporting its identity as a steady structure in zebrafish larvae (Figure 6D). Surprisingly, this system was absent in *bloc1s1*^{ihb815} at all stages examined (Figure 6D), indicating an essential role for *bloc1s1* in the formation of the surfactant system.

Since the surfactant system had never been characterized in zebrafish, we stained cryosections to obtain a better view of its organization (Figure 6E). Unexpectedly, Oil Red O staining showed that the surfactant system seemed to consist of multiple layers around the swimbladder wall, in contrast to our hypothesis that it should mimic the system in the mammalian alveolus, which consists of a single layer inside the alveolus lumen (Figure 6E). *bloc1s1*^{ihb815} larvae did not exhibit any staining, although the cryosections showed stronger staining compared with the whole mount in WT (Figure 6, D and E).

Ultrastructural defects in the swimbladder in bloc1s1^{ihb815} *larvae*

To illuminate the formation of the surfactant system in zebrafish and ultrastructural defects in the swimbladder in *bloc1s1*^{ihb815}, we performed TEM analysis during the development of the surfactant system (Figure 7).

The surfactant formed before swimbladder inflation at 4 dpf (Figure 6, D and E). The global structure of the swimbladder was similar between WT and *bloc1s1*^{ihb815} larvae at

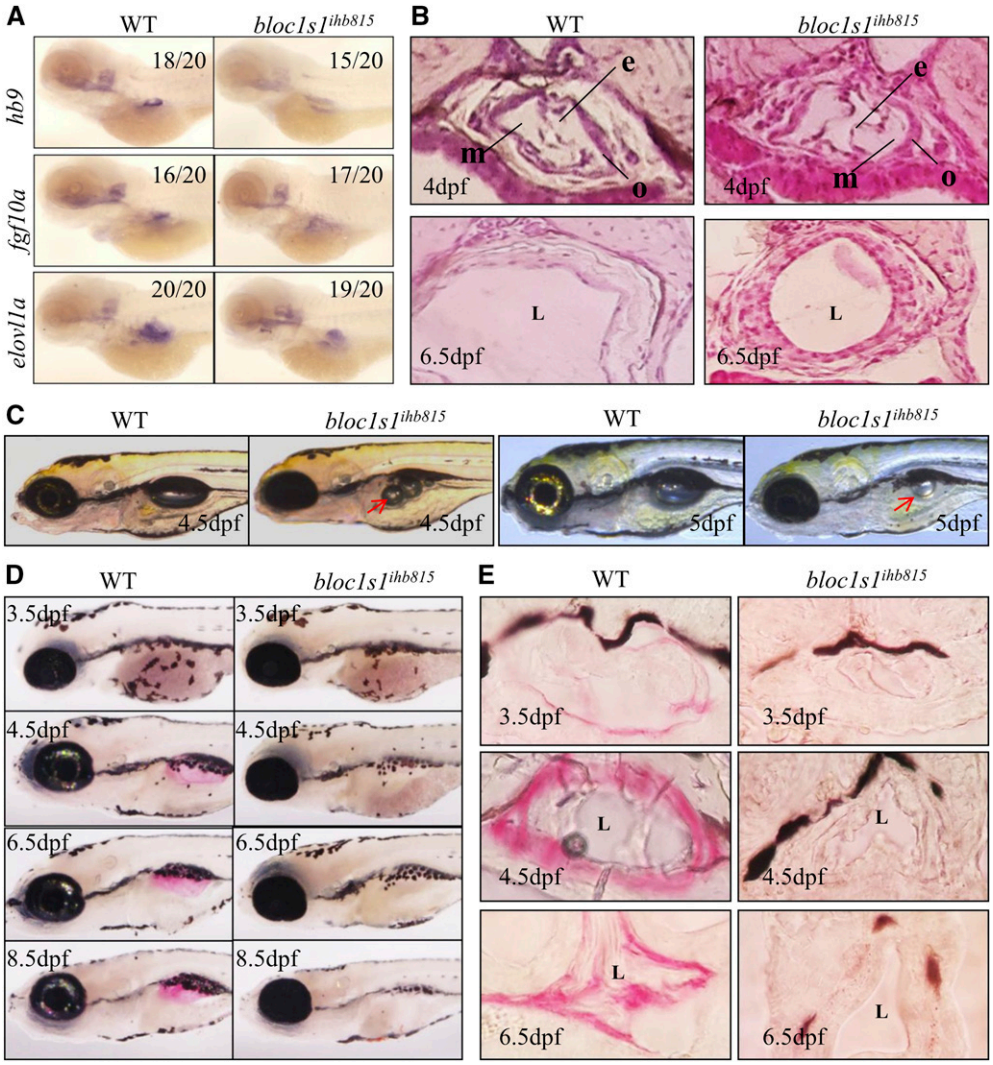

Figure 6 The surfactant system is absent in *bloc1s1*^{ihb815} zebrafish. (A) The expression of *hb9* (epithelium), *fgf10a* (mesenchyme) and *elovl1a* (outer mesothelium) in the swimbladder of WT and *bloc1s1*^{ihb815} larvae at 3.5 dpf. (B) Cross-sections of the swimbladder stained with hematoxylin in WT and *bloc1s1*^{ihb815} larvae. e, epithelium; m, mesenchyme; o, outer mesothelium. L, lumen. (C) *bloc1s1*^{ihb815} larvae possess air bubbles (arrowheads) in the gut and/or swimbladder during a period when zebrafish first inflate their swimbladder. (D) Whole-mount Oil Red O staining of WT and *bloc1s1*^{ihb815} larvae. (E) Cross cryosections (30 μm) of the swimbladder from WT and *bloc1s1*^{ihb815} larvae stained with Oil Red O. L, lumen.

that time (Figure 6B and Figure 7, A and B); it consisted of the innermost epithelium, the outermost mesothelium, and the mesenchyme located between them (Winata *et al.* 2009; Figure 7, A and B). The epithelium spread and contacted the mesothelium, and an advanced membrane system with high secretion activity formed at the site of contact (Figure 7, A and B and Figure S4, A and B in File S1). The surfactant system, corresponding to the Oil Red O staining structure in Figure 6E, existed as compact linear films between adjacent cell layers of the mesothelium (Figure 7A′). These compact linear films were absent in *bloc1s1*^{ihb815} (Figure 7B′).

After formation of the surfactant system, the swimbladder inflates and comprises multiple separate tissue layers in WT larvae at 5.5 dpf (Figure 7C). The surfactant system residing in the middle of the adjacent layers deforms on the structures (Figure 7E); this remodeling of the surfactant structure might be necessary for normal inflation. However, the developmental process is highly blocked in *bloc1s1*^{ihb815}, leading to three poorly developed tissues (epithelium, mesenchyme, and mesothelium), and the accumulation of many vesicles in the swimbladder (Figure 7D).

At 7 dpf, morphology of the cells further changed in the swimbladder, and the surfactant system presented as irregular appendages of this organ in WT (Figure 7F). The development of the swimbladder was attenuated and only formed a lumen in *bloc1s1*^{ihb815} (Figure 6B and Figure 7G). Remarkably, its inner cell layer accumulated numerous vesicles, the majority of which were empty. Some vesicles, however, contained concentric lamellae, a typical morphological feature of the lamellar body of alveolar type 2 epithelial cells. These vesicles are likely to be lamellar bodies at different immature stages (Figure 7H and Figure S4C in File S1).

Coincident with the developmental delay during the post-embryonic stages, we found that *fbp2*, a gene expressed in the swimbladder at 4.5 dpf in WT, maintained high expression at 7 dpf in *bloc1s1*^{ihb815} (Figure 7I).

Misregulation of the transcriptional network in the swimbladder of bloc1s1^{ihb815} *larvae*

As shown above, the swimbladder defect only appeared in the *bloc1s1* mutant, which is not dependent on the LRO biogenesis complex (BLOC-1) or lysosome positioning complex

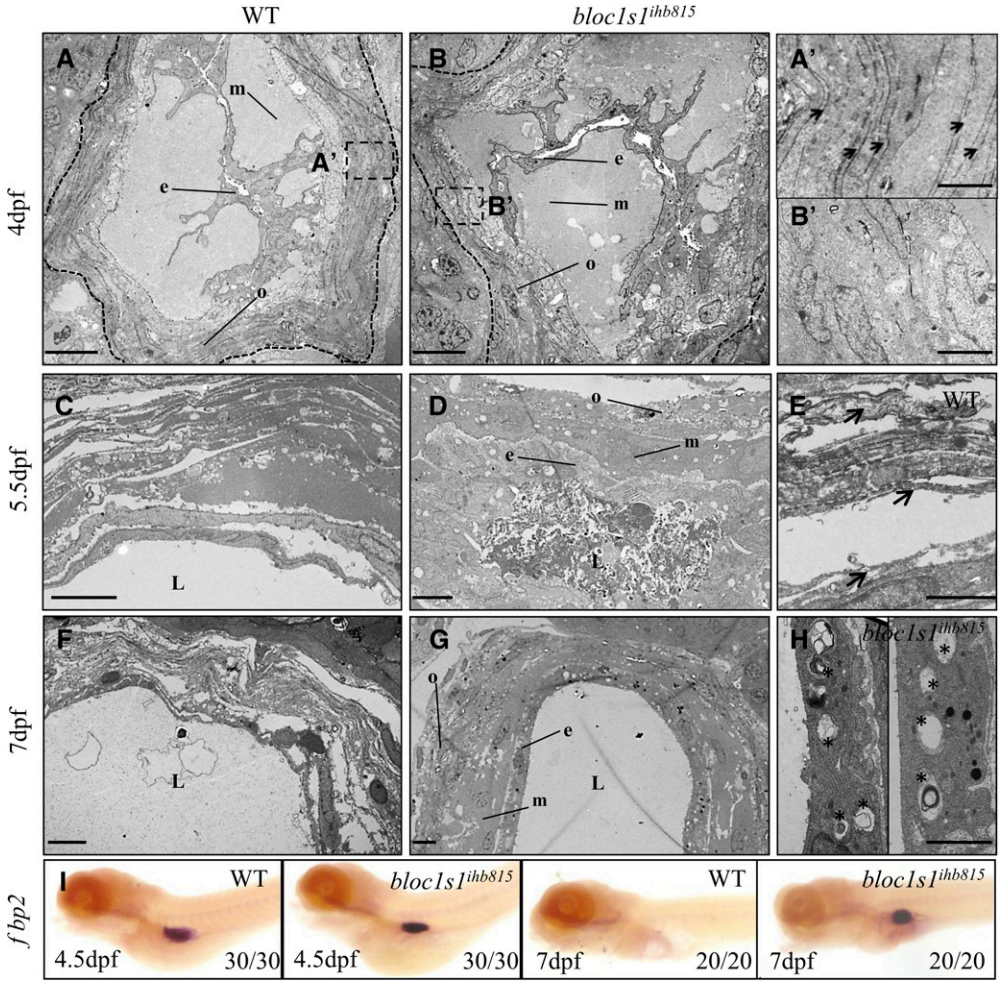

Figure 7 Ultrastructural defects in the swimbladder in *bloc1s1*^{ihb815} larvae. (A–H) TEM images of the swimbladder from WT and *bloc1s1*^{ihb815} larvae at 4 dpf (A and B), 5.5 hpf (C–E) and 7 dpf (F–H). The surfactant system exists as compact linear films between adjacent cell layers in WT larvae at 4 dpf (A′, arrowheads) and undergoes structural remodeling during development (E, arrowheads; F). The development of the *bloc1s1*^{ihb815} swimbladder at poststages is impaired (D and G). The surfactant system is lost in *bloc1s1*^{ihb815} larvae (B′, D, and G). Lamellar body-like organelles accumulate within the epithelium of the *bloc1s1*^{ihb815} swimbladder at 7 dpf (H, asterisks). e, epithelium; m, mesenchyme; o, outer mesothelium; L, lumen. Bar, 10 μm in (A and B); 5 μm in (C, D, F, and G); 2 μm in (A′, B′, E, and H). Dotted lines outlined swimbladder (A and B). (I) An early swimbladder expressed gene, *fbp2*, maintains its expression in *bloc1s1*^{ihb815} larvae at 7 dpf.

(BORC). Since BLOS1 has been reported to influence the expression of *tfeb* and *pgc1a* in mouse MEF cells (Scott *et al.* 2014), we further determined whether BLOS1 plays a role in the control of the transcriptional network that governs normal development and surfactant production in the swimbladder.

To elucidate the role of *bloc1s1* in this process, we performed *in situ* hybridization to analyze the expression of several key components involved in lung surfactant formation. These proteins include Abca3, which transports surfactant lipids into the lamellar body, Nkx2.1 (which is known to be expressed in the zebrafish swimbladder)—a key transcription factor in early lung development that regulates Abca3 and surfactant proteins expression (Whitsett and Weaver 2015)—and two key enzymes that govern surfactant lipid synthesis: Chka and Pcyt1a (Perez-Gil and Weaver 2010). Homologs of these components in zebrafish display high amino acid identity to their human counterparts (Table S2 in File S1). All of these factors were expressed in the swimbladder when the surfactant is forming at 4 dpf, and their expression levels were all strongly reduced in *bloc1s1*^{ihb815} (Figure 8A). Some of these components, such as *Nkx2.1* and *Pcyt1a*, were duplicated in the zebrafish genome, and, hence, both duplicated copies were analyzed (Figure 8A). These results, combined with our observations of the lamellar body-like organelles (Figure 7H and Figure S4C in File S1), implied that zebrafish likely shared conserved molecular mechanisms and cellular processes with mammals regulating the production of surfactant.

Multiple signaling pathways, including FGF, BMP, SHH, and WNT, have been demonstrated to play essential roles in early lung morphogenesis (Whitsett *et al.* 2015); it is possible that those signaling pathways also function in the subsequent development of lung. Moreover, some of them have been reported to regulate *NKX2.1* expression, and, thus, to influence surfactant production (Hines and Sun 2014; Luo *et al.* 2016). The requirement for SHH and WNT in zebrafish early swimbladder development has also been confirmed (Winata *et al.* 2009; Yin *et al.* 2011). Hence, we analyzed the activity of these pathways based on their respective marker genes, including *lef1* and *axin2* for WNT (Sang *et al.* 2014), *patch1* and *patch2* for SHH (Winata *et al.* 2009), and *spry4* for FGF and *ved* for BMP (Yang *et al.* 2015). Notably, the expression of all these marker genes was detected in the swimbladder of WT zebrafish at 4 dpf, and their expression levels were strongly reduced in *bloc1s1*^{ihb815} (Figure 8B), indicating that all these pathways were repressed in the *bloc1s1*^{ihb815} mutant.

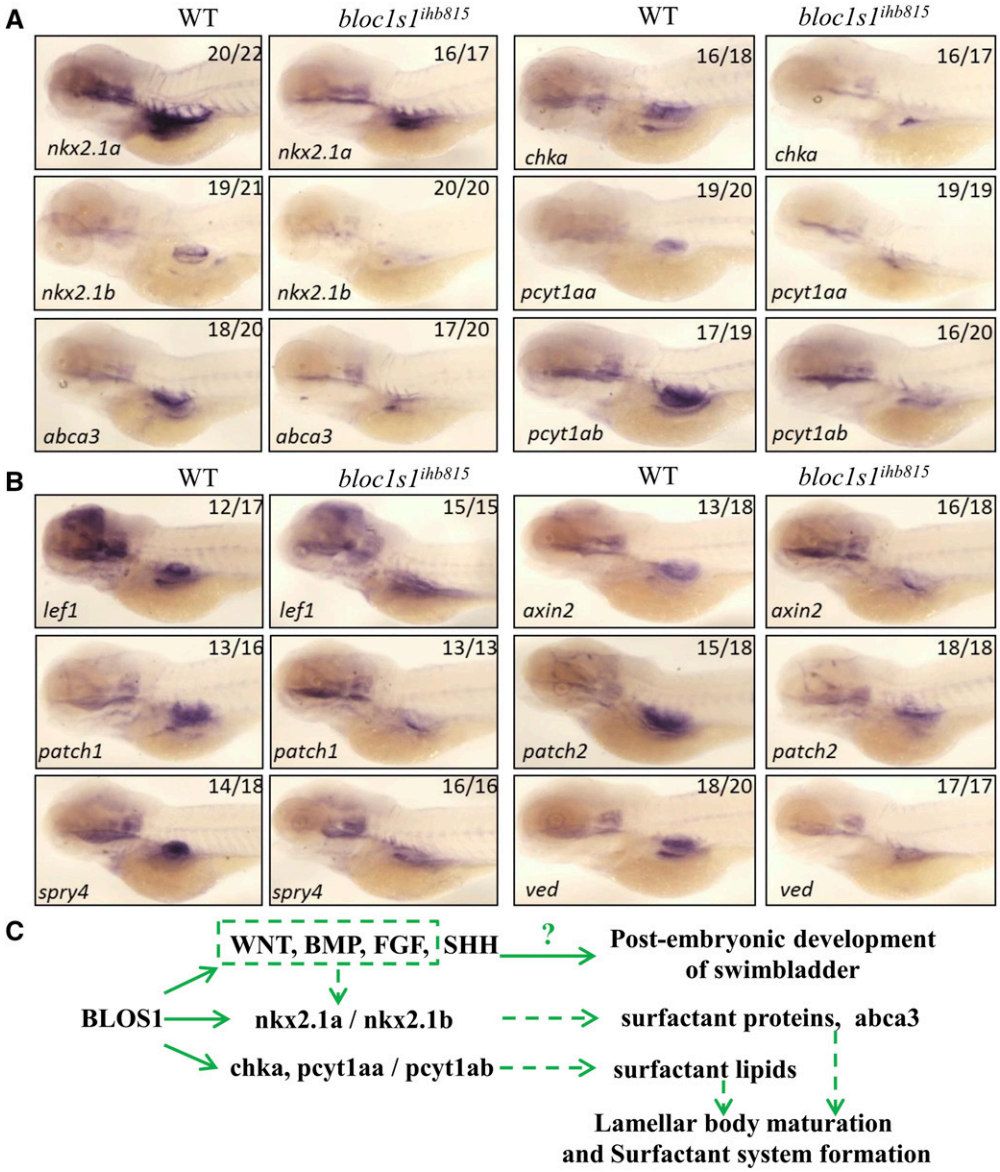

Figure 8 Misregulation of the transcriptional network in the swimbladder of *bloc1s1*^{ihb815} larvae. (A) Whole-mount *in situ* hybridization in 4 dpf embryos with probes for surfactant formation-related genes (*nkx2.1a*/*nkx2.1b*, *abca3*, *chka*, and *pcyt1aa*/*pcyt1ab*). (B) Whole-mount *in situ* hybridization in 4 dpf embryos with probes for Wnt signaling pathway genes (*lef1* and *axin2*), Shh signaling pathway genes (*patch1* and *patch2*), *spry4* for FGF, and *ved* for BMP signaling pathways. (C) The proposed model shows the function of BLOS1 in the swimbladder. The dotted lines show the pathways identified in mammals (Cheong *et al.* 2007; Goss *et al.* 2013; Hines and Sun 2014; Luo *et al.* 2016), which may be conserved in zebrafish. The question mark proposes a possible connection between these signaling pathways and the postembryonic development of the swimbladder.

Considering these results together, we conclude that the swimbladder defects in *bloc1s1*^{ihb815}larvae are caused, at least partially, by the extensive misregulation of the transcriptional network in the swimbladder.

Transgenic rescue and morpholino phenocopy of bloc1s1^{ihb815} *zebrafish phenotypes*

To finally confirm that the *bloc1s1* deletion underlies our observed phenotypes, we performed rescue experiments. We cloned the *bloc1s1* CDS-containing segment into a *Tol2* transposase destination vector and coinjected this vector with *Tol2* mRNA into single-cell embryos; this strategy partially rescued the pigment and surfactant defects in the *bloc1s1*^{ihb815} larvae (Figure S5A in File S1).

As *bloc1s1* is maternally expressed (Figure 1B), we also designed an antisense morpholino against the region containing the start codon (ATG) to evaluate the maternal effect. The injection of low concentrations of the morpholino did not obviously interfere with pigmentation or development; injection of a high dosage (7.5 ng/embryo) did not disrupt early development, but it did lead to an absence of surfactant and pigment defects, thus recapitulating the *bloc1s1*^{ihb815} phenotype (Figure S5B in File S1). This finding also indicated that maternally supplied *bloc1s1* mRNA had no additional functions in zebrafish early embryogenesis.

Discussion

Some proteins may participate in several different protein complexes, which makes it challenging to dissect their detailed functions. BLOS1 is known as a shared subunit of BLOC-1 and BORC, two distinct complexes that control LRO biogenesis and lysosome positioning, respectively (Zhang *et al.* 2014; Pu *et al.* 2015). It has also been named GCN5L1, a component of the mitochondrial acetyltransferase machinery that controls mitochondrial biogenesis and mitophagy (Scott *et al.* 2014).

In addition, the lethal phenotype of the BLOS1 mutant mouse further complicates the exploration of its functions *in vivo*. In this study, we generated and compared three zebrafish mutant lines targeting two BLOC-1 and BORC shared genes, *bloc1s1* and *bloc1s2*, and one BLOC-1 specific gene, *dtnbp1a*. We confirmed the function of BLOC-1 in LRO biogenesis during zebrafish pigmentation, and discovered that BORC regulates the positioning of lysosomal vesicles at the posterior part of the tectum. Moreover, we explored an essential role of BLOS1 in the control of surfactant formation.

The *bloc1s1*^{ihb815}, *bloc1s2*^{ihb818}, and *dtnbp1a*^{ihb819} larvae displayed reduced melanin levels that resembled those documented for BLOC-1-deficient mice and human patients (Li *et al.* 2003; Zhang *et al.* 2014; Zhou *et al.* 2016), suggesting a conserved role of BLOC-1 in melanosome biogenesis, and, thereby, making them new HPS models. Although absent in mammals, iridophores have iridosomes that contain crystallized purines, also termed silver pigment, which stack into plates and reflect light in zebrafish (Schonthaler *et al.* 2007); this pigment is also affected in *bloc1s1*^{ihb815}, *bloc1s2*^{ihb818}, and *dtnbp1a*^{ihb819} larvae (Figure 2 and Figure 5). Simultaneous melanin and silver pigment defects have also been reported in other zebrafish lines, with the mutation of genes from vesical traffic complexes such as HOPS (Maldonado *et al.* 2006; Schonthaler *et al.* 2007; Thomas *et al.* 2011) and BLOC2 (Daly *et al.* 2013). Hence, iridophores and melanocytes may employ a common pathway to control the biogenesis of their respective LROs. However, yellow pigment, which is stored in the xanthosome of xanthopores appeared to be unaffected in our mutants, indicating a different mechanism of xanthosome biogenesis. Variation in the degree of the pigment phenotype from mutants of different subunits within a complex has been documented (Li *et al.* 2004). This also occurred in *bloc1s1*^{ihb815}, *bloc1s2*^{ihb818}, and *dtnbp1a*^{ihb819}. The varied influence on melanin and silver pigment in these mutants could be explained by the fact that BLOS1 plays a key role in maintaining BLOC-1 complex stability, and thus its mutation results in the most severe pigment defect. While the silver pigment is greatly affected after BLOC-1 deficiency, the melanin defect is slight, potentially due to the different steps of BLOC-1 involvement in the development of their stored organelles. As evidenced and shown in Figure 3, BLOC-1 participates in the maturation process of melanosomes instead of the initiation of iridosome biogenesis.

The specific accumulation of Lysotracker red signals at the posterior part of the tectum occurred at the same time, and in the same region, in *bloc1s1*^{ihb815} and *bloc1s2*^{ihb818} larvae, strongly suggesting that both proteins are involved in the same process. This defect is not the main cause of lethality in *bloc1s1*^{ihb815} since *bloc1s2*^{ihb818} larvae carrying this impairment are viable. The ultrastructural features of these signals resemble perinuclear lysosome clusters in HeLa cell with a BORC deficiency, and their staining by Lysotracker red indicates that they possess lysosomal vesicle feature, namely an acidic lumen environment. Combined with the absence of these signals in *dtnbp1a*^{ihb819} larvae, of which the encoding protein is a BLOC-1 specific subunit, we propose this phenomenon implies a BORC-specific function in zebrafish larvae. BORC may be required for normal trafficking of these lysosomal vesicles in the tectum. Classical lysosomes are universal organelles that reside in most cells, but how the specific clustering of these lysosomal vesicles occurs in the tectum remains unknown, raising the following questions: what is the nature of these vesicles and their functions in the tectum, and how does BORC regulate them? Clearly, insufficient information is available to answer these questions, mandating further research. Undoubtedly, zebrafish is a powerful tool to resolve the functions of BORC *in vivo*.

BLOS1 mutant flies display abnormal glutamatergic transmission and behavior (Cheli *et al.* 2010). BLOS1 neuron-specific knockout mice are embryonic lethal like the null mutant, indicating an essential role of BLOS1 in the nervous system (Zhang *et al.* 2014). Autophagosomes accumulation is observed in BLOS1-KO MEF cells, which could contribute to developmental defects or a lethal phenotype (Zhang *et al.* 2014). BLOS2-KO mice show a variety of developmental defects, including a smaller brain size (Zhou *et al.* 2016). In contrast, we observed neither obvious nervous system-related phenotypes in either *bloc1s1*^{ihb815} or *bloc1s2*^{ihb818} larvae, nor abnormal autophagy activity in *bloc1s1*^{ihb815}, and both mutants behaved normally like their WT siblings at early stages. It is possible that these phenotype-related processes involving BLOS1 and/or BLOS2 are not conserved among vertebrates. Alternatively, subtle defects may be present that cannot be detected without sensitive assays. Indeed, increased hematopoietic stem and progenitor cell production both occur in BLOS2-KO mice and *bloc1s2* hypomorphic mutant zebrafish (Zhou *et al.* 2016), although this mutant fish was indistinguishable from WT larvae in our initial observations.

By comparing the three mutant lines, we identified BLOS1-specific (independent of BLOC-1 and BORC) phenotypes in zebrafish, expanding our knowledge of the functions of BLOS1 in vertebrates. We revealed herein an essential role of BLOS1 in surfactant formation and postembryonic development of the swimbladder. Consistent with the time that the defects appeared and progressed in *bloc1s1*^{ihb815} larvae, *bloc1s1* transcripts were highly expressed in the postembryonic stages of the swimbladder. Since the organization of the swimbladder seemed normal in *bloc1s1*^{ihb815} at 4 dpf during surfactant production, the blockage of surfactant production should have occurred prior to the postembryonic defect in the swimbladder, hence excluding a secondary effect. We performed, for the first time, a detailed characterization of the surfactant system in zebrafish larvae. The time at which it formed (around the first inflation of the swimbladder) was comparable to the time in mammals when the perinatal fetus secretes pulmonary surfactant into the alveolar space to prepare for the initial expansion and breath of the alveolus. In contrast to mammals, the surfactant of zebrafish covers each side of the tissue layers of the swimbladder wall, and undergoes structural remodeling, as shown in our TEM sections, along with postembryonic development (Figure 7). As the swimbladder wall

consists of multiple separate layers, this distribution of surfactant may function in facilitating the relative shift of different tissue layers when the swimbladder regulates its volume. Thus, its absence in *bloc1s1*^{ihb815} could impede inflation. Swimbladder deflation is a common phenotype in a variety of zebrafish mutant lines with early developmental defects (Maldonado *et al.* 2006; Thomas *et al.* 2011; Boglev *et al.* 2013). However, it is impossible that all these are related to the surfactant system, as the normal functions of nervous system and muscular system are also required for swimbladder inflation (Winata *et al.* 2010). Hence, we proposed a criteria for surfactant-specific defects in zebrafish larvae: (1) normal early swimbladder development forming three layers at 4 dpf; (2) normal nervous and muscular system development, which could be primarily judged based on their behavior and ability to deliver gas when the swimbladder first inflates; (3) negative Oil Red O staining.

The secretion of surfactant from lamellar bodies at the caudal tip of the epithelium of the adult zebrafish swimbladder has been previously reported (Robertson *et al.* 2014). Given the obvious different ultrastructures between zebrafish adult and larval swimbladders (Figure 7; Robertson *et al.* 2014), it must undergo continuous development and reorganization. Although we did not observe these lamellar body-like organelles in WT zebrafish larvae during surfactant formation, it is possible that there is a specific area, as in the adult zebrafish, to execute this function that was not present in our TEM sections. Interestingly, in the late stages, these lamellar body-like organelles were found in the *bloc1s1*^{ihb815} epithelium (Figure 7H and Figure S4C in File S1), but most of them were in an immature state. Hence, another possible explanation is that lamellar bodies formation and secretion occurs quickly during surfactant production, which makes it difficult to capture them in WT sections, and defects in their formation result in immature lamellar bodies, which block their normal secretion and progressive accumulation in the *bloc1s1*^{ihb815} epithelium, allowing their observation. The advanced membrane system at the contact site of the epithelium and mesothelium implies that surfactant could be secreted into the mesoslim spaces from these junctions (Figure S4, A and B in File S1). In addition to *NKX2.1*, the expression of which in the swimbladder has been previously reported (Cass *et al.* 2013), we detected high expression levels of several key components involved in lung surfactant production in the swimbladder of zebrafish during surfactant formation, including *ABCA3*, *CHKA*, and *PCYT1* (Figure 8A). These results strongly suggest that zebrafish and mammals share, at least to some extent, conserved molecular and cellular processes that regulate the production of surfactant, and that an insufficient supply of these factors could underlie the surfactant shortage/absence in *bloc1s1*^{ihb815}. WNT, SHH, FGF, and BMP signaling pathways have been extensively studied in early lung morphogenesis, and the requirement for SHH and WNT in zebrafish early swimbladder development has also been confirmed (Winata *et al.* 2009; Yin *et al.* 2011). Moreover, some of them have been reported to regulate lung surfactant production (Hines and Sun 2014; Luo *et al.* 2016), implying a connection between these signaling pathways and the regulation of surfactant formation. We confirmed the expression of marker genes for these signaling pathways in the swimbladder during surfactant formation, and their reduced expression after *bloc1s1* mutation (Figure 8B). Thus, the profound reduction of activity of these signaling pathways could explain, at least in part, both the surfactant and the developmental defects in the swimbladder in *bloc1s1*^{ihb815} (Figure 8C). Our work expands our knowledge concerning the similarities between the swimbladder and lung, and reveals the potential value of zebrafish for surfactant biology research.

Acknowledgments

This work was supported by grants from the Chinese Academy of Sciences (grant KJZD-EW-L08), Hi-Tech Research and Development Program of China (863 Program, 2012AA022402-Y312021603) and from National Natural Science Foundation of China (Grants 31371354 and 31400654). The authors declare no conflict of interest.

Literature Cited

Ammann, S., A. Schulz, I. Krageloh-Mann, N. M. Dieckmann, K. Niethammer *et al.*, 2016 Mutations in AP3D1 associated with immunodeficiency and seizures define a new type of Hermansky-Pudlak syndrome. Blood 127: 997–1006.

Boglev, Y., A. P. Badrock, A. J. Trotter, Q. Du, E. J. Richardson *et al.*, 2013 Autophagy induction is a Tor- and Tp53-independent cell survival response in a zebrafish model of disrupted ribosome biogenesis. PLoS Genet. 9: e1003279.

Bultema, J. J., A. L. Ambrosio, C. L. Burek, and S. M. Di Pietro, 2012 BLOC-2, AP-3, and AP-1 proteins function in concert with Rab38 and Rab32 proteins to mediate protein trafficking to lysosome-related organelles. J. Biol. Chem. 287: 19550–19563.

Cai, Q., L. Lu, J.-H. Tian, Y.-B. Zhu, H. Qiao *et al.*, 2010 Snapin-regulated late endosomal transport is critical for efficient autophagy-lysosomal function in neurons. Neuron 68: 73–86.

Cass, A. N., M. D. Servetnick, and A. R. McCune, 2013 Expression of a lung developmental cassette in the adult and developing zebrafish swimbladder. Evol. Dev. 15: 119–132.

Chang, N., C. Sun, L. Gao, D. Zhu, X. Xu *et al.*, 2013 Genome editing with RNA-guided Cas9 nuclease in zebrafish embryos. Cell Res. 23: 465–472.

Cheli, V. T., R. W. Daniels, R. Godoy, D. J. Hoyle, V. Kandachar *et al.*, 2010 Genetic modifiers of abnormal organelle biogenesis in a Drosophila model of BLOC-1 deficiency. Hum. Mol. Genet. 19: 861–878.

Cheong, N., H. Zhang, M. Madesh, M. Zhao, K. Yu *et al.*, 2007 ABCA3 is critical for lamellar body biogenesis in vivo. J. Biol. Chem. 282: 23811–23817.

Ciciotte, S. L., B. Gwynn, K. Moriyama, M. Huizing, W. A. Gahl *et al.*, 2003 Cappuccino, a mouse model of Hermansky-Pudlak syndrome, encodes a novel protein that is part of the pallidin-muted complex (BLOC-1). Blood 101: 4402–4407.

Cullinane, A. R., J. A. Curry, C. Carmona-Rivera, C. G. Summers, C. Ciccone *et al.*, 2011 A BLOC-1 mutation screen reveals that PLDN is mutated in Hermansky-Pudlak syndrome type 9. Am. J. Hum. Genet. 88: 778–787.

Cullinane, A. R., J. A. Curry, G. Golas, J. Pan, C. Carmona-Rivera *et al.*, 2012 A BLOC-1 mutation screen reveals a novel BLOC1S3 mutation in Hermansky-Pudlak syndrome type 8. Pigment Cell Melanoma Res. 25: 584–591.

Daly, C. M., J. Willer, R. Gregg, and J. M. Gross, 2013 snow white, a zebrafish model of Hermansky-Pudlak syndrome type 5. Genetics 195: 481–494.

Daniels, C. B., and S. Orgeig, 2003 Pulmonary surfactant: the key to the evolution of air breathing. News Physiol. Sci. 18: 151–157.

Di Giovanni, J., and Z. H. Sheng, 2015 Regulation of synaptic activity by snapin-mediated endolysosomal transport and sorting. EMBO J. 34: 2059–2077.

Di Pietro, S. M., J. M. Falcon-Perez, D. Tenza, S. R. Setty, M. S. Marks *et al.*, 2006 BLOC-1 interacts with BLOC-2 and the AP-3 complex to facilitate protein trafficking on endosomes. Mol. Biol. Cell 17: 4027–4038.

Goss, V., A. N. Hunt, and A. D. Postle, 2013 Regulation of lung surfactant phospholipid synthesis and metabolism. Biochim. Biophys. Acta 1831: 448–458.

Gratacap, R. L., J. F. Rawls, and R. T. Wheeler, 2013 Mucosal candidiasis elicits NF- B activation, proinflammatory gene expression and localized neutrophilia in zebrafish. Dis. Model. Mech. 6: 1260–1270.

Gu, Q., X. Yang, L. Lin, S. Li, Q. Li *et al.*, 2014 Genetic ablation of solute carrier family 7a3a leads to hepatic steatosis in zebrafish during fasting. Hepatology 60: 1929–1941.

Herriges, M., and E. E. Morrisey, 2014 Lung development: orchestrating the generation and regeneration of a complex organ. Development 141: 502–513.

Hines, E. A., and X. Sun, 2014 Tissue crosstalk in lung development. J. Cell. Biochem. 115: 1469–1477.

Hugo, S. E., L. Cruz-Garcia, S. Karanth, R. M. Anderson, D. Y. Stainier *et al.*, 2012 A monocarboxylate transporter required for hepatocyte secretion of ketone bodies during fasting. Genes Dev. 26: 282–293.

Huizing, M., A. Helip-Wooley, W. Westbroek, M. Gunay-Aygun, and W. A. Gahl, 2008 Disorders of lysosome-related organelle biogenesis: clinical and molecular genetics. Annu. Rev. Genomics Hum. Genet. 9: 359–386.

Ilardi, J. M., S. Mochida, and Z. H. Sheng, 1999 Snapin: a SNARE-associated protein implicated in synaptic transmission. Nat. Neurosci. 2: 119–124.

Korzh, S., X. Pan, M. Garcia-Lecea, C. Winata, X. Pan *et al.*, 2008 Requirement of vasculogenesis and blood circulation in late stages of liver growth in zebrafish. BMC Dev. Biol. 8: 84.

Li, W., Q. Zhang, N. Oiso, E. K. Novak, R. Gautam *et al.*, 2003 Hermansky-Pudlak syndrome type 7 (HPS-7) results from mutant dysbindin, a member of the biogenesis of lysosome-related organelles complex 1 (BLOC-1). Nat. Genet. 35: 84–89.

Li, W., M. E. Rusiniak, S. Chintala, R. Gautam, E. K. Novak *et al.*, 2004 Murine Hermansky-Pudlak syndrome genes: regulators of lysosome-related organelles. BioEssays 26: 616–628.

López Hernández, Y., D. Yero, J. M. Pinos-Rodríguez, and I. Gibert, 2015 Animals devoid of pulmonary system as infection models in the study of lung bacterial pathogens. Front. Microbiol. 6: 38.

Luo, Y., H. Chen, S. Ren, N. Li, Y. Mishina *et al.*, 2016 BMP signaling is essential in neonatal surfactant production during respiratory adaptation. Am. J. Physiol. Lung Cell. Mol. Physiol. 311: L29–L38.

Maldonado, E., F. Hernandez, C. Lozano, M. E. Castro, and R. E. Navarro, 2006 The zebrafish mutant vps18 as a model for vesicle-traffic related hypopigmentation diseases. Pigment Cell Res. 19: 315–326.

Malicki, J., A. Avanesov, J. Li, S. Yuan, and Z. Sun, 2011 Analysis of cilia structure and function in zebrafish. Methods Cell Biol. 101: 39–74.

Marks, M. S., H. F. G. Heijnen, and G. Raposo, 2013 Lysosome-related organelles: unusual compartments become mainstream. Curr. Opin. Cell Biol. 25: 495–505.

Morgan, N. V., S. Pasha, C. A. Johnson, J. R. Ainsworth, R. A. Eady *et al.*, 2006 A germline mutation in BLOC1S3/reduced pigmentation causes a novel variant of Hermansky-Pudlak syndrome (HPS8). Am. J. Hum. Genet. 78: 160–166.

Newell-Litwa, K., G. Salazar, Y. Smith, and V. Faundez, 2009 Roles of BLOC-1 and adaptor protein-3 complexes in cargo sorting to synaptic vesicles. Mol. Biol. Cell 20: 1441–1453.

Olmeda, B., M. Martínez-Calle, and J. Pérez-Gil, 2017 Pulmonary surfactant metabolism in the alveolar airspace: biogenesis, extracellular conversions, recycling. Ann. Anat. 209: 78–92.

Perez-Gil, J., and T. E. Weaver, 2010 Pulmonary surfactant pathophysiology: current models and open questions. Physiology (Bethesda) 25: 132–141.

Pu, J., C. Schindler, R. Jia, M. Jarnik, P. Backlund *et al.*, 2015 BORC, a multisubunit complex that regulates lysosome positioning. Dev. Cell 33: 176–188.

Robertson, G. N., R. P. Croll, and F. M. Smith, 2014 The structure of the caudal wall of the zebrafish (Danio rerio) swim bladder: evidence of localized lamellar body secretion and a proximate neural plexus. J. Morphol. 275: 933–948.

Salazar, G., B. Craige, M. L. Styers, K. A. Newell-Litwa, M. M. Doucette *et al.*, 2006 BLOC-1 complex deficiency alters the targeting of adaptor protein complex-3 cargoes. Mol. Biol. Cell 17: 4014–4026.

Sang, Q., J. Zhang, R. Feng, X. Wang, Q. Li *et al.*, 2014 Ildr1b is essential for semicircular canal development, migration of the posterior lateral line primordium and hearing ability in zebrafish: implications for a role in the recessive hearing impairment DFNB42. Hum. Mol. Genet. 23 6201–6211.

Sasaki, T., S. Lian, J. Qi, P. E. Bayliss, C. E. Carr *et al.*, 2014 Aberrant autolysosomal regulation is linked to the induction of embryonic senescence: differential roles of Beclin 1 and p53 in vertebrate Spns1 deficiency. PLoS Genet. 10: e1004409.

Schonthaler, H. B., V. C. Fleisch, O. Biehlmaier, Y. Makhankov, O. Rinner *et al.*, 2007 The zebrafish mutant lbk/vam6 resembles human multisystemic disorders caused by aberrant trafficking of endosomal vesicles. Development 135: 387–399.

Scott, I., B. R. Webster, J. H. Li, and M. N. Sack, 2012 Identification of a molecular component of the mitochondrial acetyltransferase programme: a novel role for GCN5L1. Biochem. J. 443: 655–661.

Scott, I., B. R. Webster, C. K. Chan, J. U. Okonkwo, K. Han *et al.*, 2014 GCN5-like protein 1 (GCN5L1) controls mitochondrial content through coordinated regulation of mitochondrial biogenesis and mitophagy. J. Biol. Chem. 289: 2864–2872.

Settembre, C., C. Di Malta, V. A. Polito, M. G. Arencibia, F. Vetrini *et al.*, 2011 TFEB links autophagy to lysosomal biogenesis. Science 332: 1429–1433.

Setty, S. R. G., D. Tenza, S. T. Truschel, E. Chou, E. V. Sviderskaya *et al.*, 2007 BLOC-1 is required for cargo-specific sorting from vacuolar early endosomes toward lysosome-related organelles. Mol. Biol. Cell 18: 768–780.

Sitaram, A., M. K. Dennis, R. Chaudhuri, W. De Jesus-Rojas, D. Tenza *et al.*, 2012 Differential recognition of a dileucine-based sorting signal by AP-1 and AP-3 reveals a requirement for both BLOC-1 and AP-3 in delivery of OCA2 to melanosomes. Mol. Biol. Cell 23: 3178–3192.

Stahlman, M. T., M. P. Gray, M. W. Falconieri, J. A. Whitsett, and T. E. Weaver, 2000 Lamellar body formation in normal and surfactant protein B-deficient fetal mice. Lab. Invest. 80: 395–403.

Thomas, J. L., T. S. Vihtelic, A. D. denDekker, G. Willer, X. Luo *et al.*, 2011 The loss of vacuolar protein sorting 11 (vps11) causes retinal pathogenesis in a vertebrate model of syndromic albinism. Invest. Ophthalmol. Vis. Sci. 52: 3119–3128.

Tian, J. H., Z. X. Wu, M. Unzicker, L. Lu, Q. Cai *et al.*, 2005 The role of snapin in neurosecretion: snapin knock-out mice exhibit impaired calcium-dependent exocytosis of large dense-core vesicles in chromaffin cells. J. Neurosci. 25: 10546–10555.

Voelz, K., R. L. Gratacap, and R. T. Wheeler, 2015 A zebrafish larval model reveals early tissue-specific innate immune responses to Mucor circinelloides. Dis. Model. Mech. 8: 1375–1388.

Webster, B. R., I. Scott, K. Han, J. H. Li, Z. Lu *et al.*, 2013 Restricted mitochondrial protein acetylation initiates mitochondrial autophagy. J. Cell Sci. 126: 4843–4849.

Wei, A.-H., and W. Li, 2013 Hermansky-Pudlak syndrome: pigmentary and non-pigmentary defects and their pathogenesis. Pigment Cell Melanoma Res. 26: 176–192.

Whitsett, J. A., 2014 The molecular era of surfactant biology. Neonatology 105: 337–343.

Whitsett, J. A., and T. E. Weaver, 2015 Alveolar development and disease. Am. J. Respir. Cell Mol. Biol. 53: 1–7.

Whitsett, J. A., S. E. Wert, and T. E. Weaver, 2010 Alveolar surfactant homeostasis and the pathogenesis of pulmonary disease. Annu. Rev. Med. 61: 105–119.

Whitsett, J. A., S. E. Wert, and T. E. Weaver, 2015 Diseases of pulmonary surfactant homeostasis. Annu. Rev. Pathol. 10: 371–393.

Winata, C. L., S. Korzh, I. Kondrychyn, W. Zheng, V. Korzh *et al.*, 2009 Development of zebrafish swimbladder: the requirement of hedgehog signaling in specification and organization of the three tissue layers. Dev. Biol. 331: 222–236.

Winata, C. L., S. Korzh, I. Kondrychyn, V. Korzh, and Z. Gong, 2010 The role of vasculature and blood circulation in zebrafish swimbladder development. BMC Dev. Biol. 10: 3.

Wittkopp, N., E. Huntzinger, C. Weiler, J. Sauliere, S. Schmidt *et al.*, 2009 Nonsense-mediated mRNA decay effectors are essential for zebrafish embryonic development and survival. Mol. Cell. Biol. 29: 3517–3528.

Yang, Q., X. He, L. Yang, Z. Zhou, A. R. Cullinane *et al.*, 2012 The BLOS1-interacting protein KXD1 is involved in the biogenesis of lysosome-related organelles. Traffic 13: 1160–1169.

Yang, X., Q. Gu, L. Lin, S. Li, S. Zhong *et al.*, 2015 Nucleoporin 62-like protein activates canonical Wnt signaling through facilitating the nuclear import of beta-catenin in zebrafish. Mol. Cell. Biol. 35: 1110–1124.

Yin, A., S. Korzh, C. L. Winata, V. Korzh, and Z. Gong, 2011 Wnt signaling is required for early development of zebrafish swimbladder. PLoS One 6: e18431.

Yin, A., V. Korzh, and Z. Gong, 2012 Perturbation of zebrafish swimbladder development by enhancing Wnt signaling in Wif1 morphants. Biochim. Biophys. Acta 1823: 236–244.

Zhang, A., X. He, L. Zhang, L. Yang, P. Woodman *et al.*, 2014 Biogenesis of lysosome-related organelles complex-1 subunit 1 (BLOS1) interacts with sorting nexin 2 and the endosomal sorting complex required for transport-I (ESCRT-I) component TSG101 to mediate the sorting of epidermal growth factor receptor into endosomal compartments. J. Biol. Chem. 289: 29180–29194.

Zhang, Q., W. Li, E. K. Novak, A. Karim, V. S. Mishra *et al.*, 2002 The gene for the muted (mu) mouse, a model for Hermansky-Pudlak syndrome, defines a novel protein which regulates vesicle trafficking. Hum. Mol. Genet. 11: 697–706.

Zhang, Y., H. Liu, J. Yao, Y. Huang, S. Qin *et al.*, 2016 Manipulating the air-filled zebrafish swim bladder as a neutrophilic inflammation model for acute lung injury. Cell Death Dis. 7: e2470.

Zheng, W., Z. Wang, J. E. Collins, R. M. Andrews, D. Stemple *et al.*, 2011 Comparative transcriptome analyses indicate molecular homology of zebrafish swimbladder and mammalian lung. PLoS One 6: e24019.

Zhou, W., Q. He, C. Zhang, X. He, Z. Cui *et al.*, 2016 BLOS2 negatively regulates Notch signaling during neural and hematopoietic stem and progenitor cell development. eLife 10: 18108.

Communicating editor: D. Parichy